Journal of Wasit for Science and Medicine 2026: 19, (3), 144-157

Corrosion of Mild Steel in Saline Environments: Mechanisms, Influencing Factors, and Recent Mitigation Strategies

Thaqeef Murtada Jawad

thaqeef@uowasit.edu.iq
Department of chemistry, College of Science, University of Wasit, Wasit, Iraq

Abstract

Mild steel is prized because of its mechanical qualities and low prices but very vulnerable to corrosion in salty conditions such as in the marine areas. The paper examines its weight loss, potentiodynamic polarization and electrochemical impedance spectroscopy (EIS) corrosion behavior in 3.5 wt.% NaCl. Findings indicate that the rate of corrosion rises with the chloride concentration to a certain optimum and after that, the rate of oxygen diffusion begins to be limiting. High temperatures and acidic PH promote corrosion and an increase in flow velocity increases the mass transfer and promotes corrosion rates. The splash zone is the worst of all the marine zones. Recent mitigation measures are critically assessed: an environmentally-friendly organic/inorganic hybrid inhibitor has 95.75 % inhibition potential and graphene-based coating has more than 1000 hours of protection in saline conditions. Also, prediction models, based on machine learning, are talked about. The results provide very useful information to the design and maintenance of mild steel structures in coastal and marine works to overcome economic, safety and environmental challenges.

Keyword: Mild steel corrosion; Saline environment; Marine corrosion; Green inhibitors.

1. Introduction

Corrosion is a widespread and an expensive process that occurs in metallic structures in practically all industrial fields. Although mild steel is the most widely used engineering alloy due to its good balance of strength, ductility and affordability, it has a low inherent corrosion resistance especially in an environment that includes chloride ions. Cost of corrosion in the whole world is estimated to cost over two and a half trillion US dollars every year which is about three to four percent of the total world gross domestic product (GDP) [1-3]. The most aggressive corrosive environments of mild steel are salty environments such as seas, coastal environments such as the atmosphere and salt applied to de-ice. The chloride ions presence

interferes with the passive oxide layers, enhances anodic dissolution, and induces localized corrosion behavior like pitting and crevice corrosion. High salinity and moisture content in the atmosphere of island countries and coastal areas result in particularly serious atmospheric corrosion [4-6].

The aim of the study will be to carry out a comprehensive investigation on the corrosion behavior of mild steel in saline environment which will entail the basic electrochemical processes involved in the corrosion by chloride, the effect of various environmental factors including chloride concentration, temperature, pH, dissolved oxygen and flow velocity and a comparative study of the severity of corrosion in various marine environments such as atmospheric zone, splash The paper combines the experimental data of the controlled laboratory experiments with the field exposure data to present practical guidelines to be applied to corrosion control in saline conditions.

2. Experimental Methodology

2.1 Materials

Test specimens were made of mild steel coupons (AISI 1010) with size 50mm x 25mm x 3mm. The chemical composition (wt.%) was: C 0.10%, Mn 0.35%, P 0.02%, S 0.02%, and Fe balance. Specimens were ground using silicon carbide paper to a maximum of 1200 grit, then the acetone was used to degrease, followed by distilled water and finally dried before testing [7-9].

2.2 Preparation of Saline Solutions.

To prepare Saline Solutions with a concentration of 0.5 w.% of sodium chloride (NaCl) to 10 w.% were prepared in distilled water simulating the saline and marine ecosystems. Artificial seawater was made as per ASTM D1141 specifications.

2.3 Corrosion Testing Procedures

Weight Loss Technique: Sample solutions were placed in test solutions over periods of 168 hours (7 days) to 720 hours (30 days) at various controlled temperatures (25 o C -60 o C). Corrosion products were washed away after immersion in Clarke solution (500ml Hl 3.5 g hexamethylenetetramine) and weight loss was recorded with the help of a precision balance (accuracy of 0.0001g). The formula to compute the rate of corrosion in mm/year was [10-12]:

$$\mathbf{CR = (K \times \Delta W) / (A \times t \times \rho)}$$

Where; $K = 8.76 \times 10^4$, ΔW = weight loss (g), A = surface area (cm^2), t = time (h), ρ = density (7.86 g/cm^3).

Electrochemical Measurements: Potentiodynamic polarization and EIS were performed using a three- Electrode cell setup with a saturated calomel reference electrode

(SCE), platinum counter electrode, and a mild steel working electrode (1cm2 exposed area). Scans of polarization were conducted at 1mV/s between -250mV and +250mV against OCP. At OCP, EIS measurements were made over the frequency range of 105Hz to 10 -2Hz at an AC amplitude of 10mV [12-14].

2.4 Surface Characterization

Scanning electron microscopy (SEM) with energy-dispersive X-ray spectroscopy (EDS) were used to study surface morphology and compositions of corrosion products. Phases of corrosion products (lepidocrocite 7-FeOOH, goethite 7-FeOOH, magnetite Fe_3O_4) were identified with the help of Raman spectroscopy and X-ray diffraction (XRD) [14-16].

3. Results and discussion

The objectives of the experiment were to determine the effect of chloride concentration on the rate of corrosion. The corrosion characteristics of mild steel were studied in NaCl solutions of 0.5, 1.0, 3.5, 5.0, and 10.0 wt.% concentration during a 168-hour immersion period. The weight loss and the calculated corrosion rates are summarized in Table 1. The rate of corrosion was also observed to increase with the concentration of NaCl up to about 5 wt.% beyond which a decrease was noted because of the diffusion of oxygen at the higher ionic strength.

This parabolic relationship is depicted in Figure 1 where the highest rate of corrosion is observed at approximately 5 wt.% NaCl [14-16].

Table 1: Effect of NaCl Concentraton on Corrosion of Mild Steel (168 h immersion ,25° C)

NaCl Concentration (wt.%)	Initial Mass (g)	Final Mass (g)	Weight Loss (g)	Corrosion Rate (mm/year)
0.5	23.4562	23.4415	0.0147	0.087
1.0	23.5123	23.4928	0.0195	0.115
3.5	23.4891	23.4612	0.0279	0.165
5.0	23.5247	23.4953	0.0294	0.174
10.0	23.4786	23.4541	0.0245	0.145

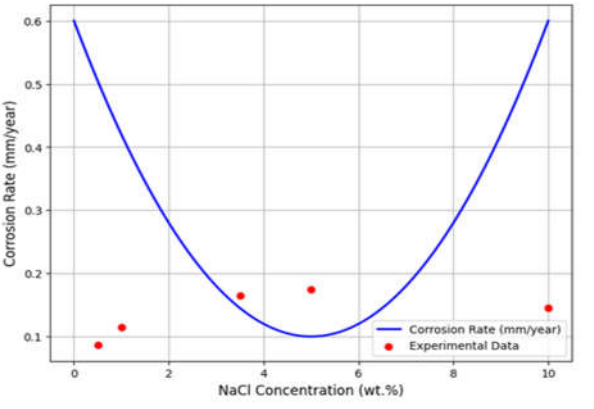

Figure 1: Corrosion Rate as a Function of NaCl Concentration – A parabolic curve showing maximum corrosion rate at approximately 5 wt.%

NaCl, with decreased rates at higher concentrations due to oxygen diffusion limitation.

3.1 Effect of Temperature on Corrosion Rate

Table 2 shows the rate of corrosion at various temperatures (25 ºC to 60 ºC) during 168 hours in 3.5 wt.% solution of NaCl. High temperatures enhanced both the anodic dissolution and oxygen reduction rate, as shown in Figure 2 (Arrhenius plot, ln CR vs. 1/T) indicating an activation energy of 28 kJ/mol of corrosion process in this saline solution [12-15].

Table 2: Effect of Temperature on Corrosion of Mild Steel in 3.5 wt.% NaCl (168 h immersion)

Temperature (°C)	Weight Loss (g)	Corrosion Rate (mm/year)
25	0.0279	0.165
35	0.0412	0.244
45	0.0587	0.347
60	0.0823	0.487

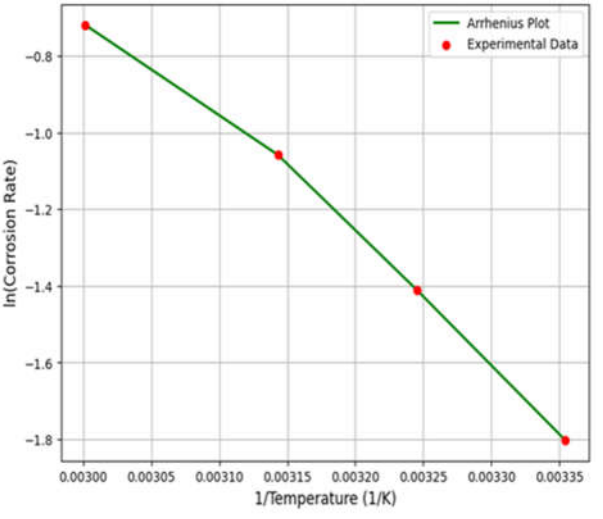

Figure 2: Arrhenius Plot of Corrosion Rate vs. Temperature – Linear relationship (ln CR vs. 1/T) confirming activation energy of 28 kJ/mol for the corrosion process in 3.5 wt.% NaCl.

3.2. Effect of pH on Corrosion Rate

Table 3 presents the results of corrosion of mild steel in 3.5 wt.% NaCl at different pH conditions (adjusted with HCl or NaOH). The rate of corrosion in acidic environments (pH 3) was more than 500 % faster than in neutral environments, whereas corrosion was slower in alkaline environments and passivation was faster. Figure 3 illustrates the sharp rise in velocity of corrosion at a pH lower than 5 and the marked decrease at a pH higher than 9 which indicate passivation in an alkaline environment [15-17].

3.3 Effect of Flow Velocity

The effect of flow velocity on the rate of corrosion was determined by rotating cylinder electrode in 3.5 wt.% NaCl at 25 C summarized in Table 4. The velocity of flow greatly enhanced the rate of corrosion; the highest rate of corrosion (4.741 mm/year) was measured at 0.3m/s, which was explained by the increased transport rate of oxygen and the removal of protective corrosion products. The exponential dependence of the corrosion rate on the flow velocity as illustrated in Figure 4 indicates the change of control regime to the diffusion-controlled regime to the activation-controlled regime [13-16].

Table 3: Effect of pH on Corrosion of Mild Steel in 3.5 wt.% NaCl (168 h, 25 °C)

pH	Weight Loss (g)	Corrosion Rate (mm/year)	Surface Observation
3.0	0.0894	0.529	Severe uniform corrosion
5.0	0.0456	0.270	Moderate corrosion
7.0	0.0279	0.165	Mild uniform corrosion
9.0	0.0153	0.091	Slight corrosion
11.0	0.0098	0.058	Minimal corrosion, passivation

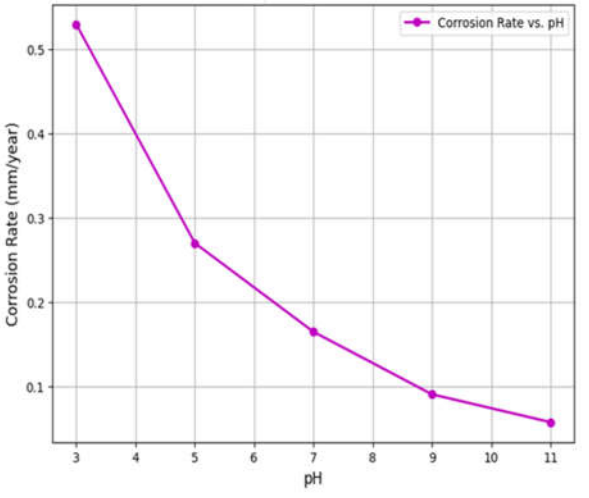

Figure 3: Effect of pH on Corrosion Rate – Steep increase in corrosion rate below pH 5 and significant reduction above pH 9, demonstrating passivation in alkaline conditions.

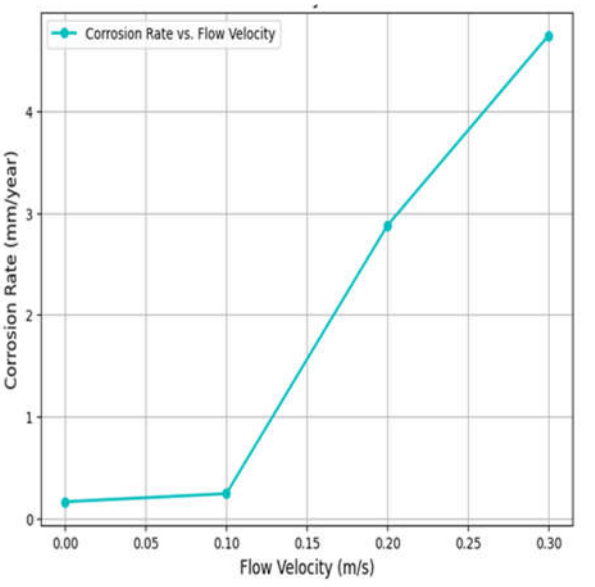

Figure 4: Flow Velocity vs. Corrosion Rate – Exponential increase in corrosion rate with flow velocity, with transition from diffusion-controlled to activation-controlled regimes.

Table 4: Effect of Flow Velocity on Corrosion of Mild Steel in 3.5 wt.% NaCl (168 h)

Flow Velocity (m/s)	**Corrosion Rate (mm/year)**
0 (Static)	0.165
0.1	0.244
0.2	2.876
0.3	4.741

3.4 Comparative Corrosion Across Marine Zones

The severity of corrosion in various areas of the marine environment was measured using the SMED apparatus and the measurements were taken after 30 days of exposure as provided in Table 5. The intensity of corrosion was the greatest in the splash zone, which is about 3.5 times higher than in the atmospheric zone, because of cyclic wetting and drying conditions that concentrate chlorides and give rise to different forms of aeration cells. Figure 5 is a bar chart that has been used to compare the rates of corrosion in the atmospheric, tidal, immersion and splash environments, which clearly shows that the splash zone is the most aggressive [14-17].

Table 5: Corrosion Loss Across Different Marine Zones (30-day exposure)

Marine Zone	**Average Weight Loss (g)**	**Corrosion Rate (mm/year)**	**Relative Severity**
Atmospheric Zone	0.0312	0.185	1.0 (Reference)
Tidal Zone	0.0528	0.312	1.69
Immersion Zone	0.0685	0.405	2.19
Splash Zone	0.1093	0.646	3.49

3.5 Electrochemical Polarization Results

Table 6 shows electrochemical parameters obtained in potentiodynamic polarization curves. Figure 6 illustrates the Tafel plots of mild steel in the presence of 3.5 wt. NaCl at different temperatures (25 -60 oC) based on which the corrosion current densities and Tafel slopes were calculated [12-14].

Table 6: Electrochemical Polarization Parameters for Mild Steel in 3.5 wt.% NaCl at 25 °C.

Parameter	Value
Corrosion Potential, E corr (mV vs. SCE)	–678 ± 12
Corrosion Current Density, I corr (μA/cm²)	18.4 ± 2.1
Anodic Tafel Slope, βa (mV/decade)	85 ± 8
Cathodic Tafel Slope, βc (mV/decade)	145 ± 12
Polarization Resistance, R p (Ω·cm²)	1280 ± 150

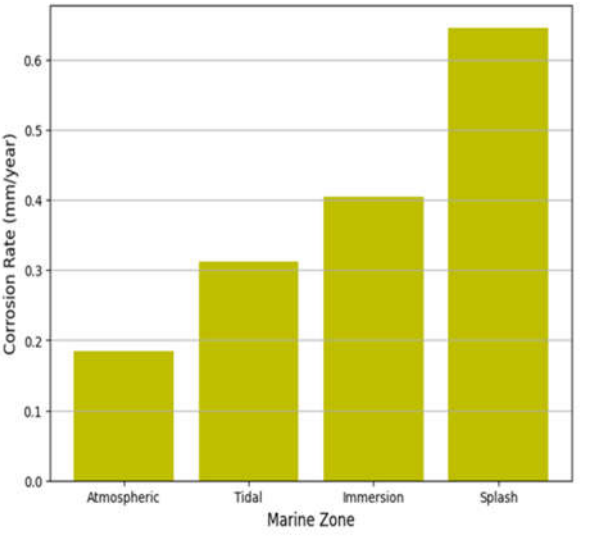

Figure 5: Comparative Corrosion Severity Across Marine Zones – Bar chart showing splash zone corrosion rate 3.5× higher than atmospheric zone.

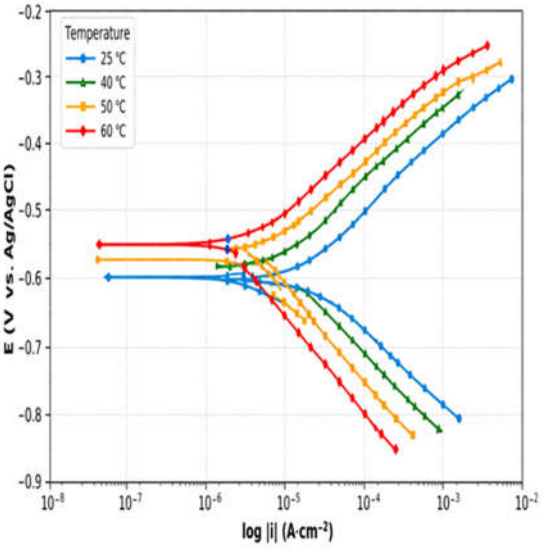

Figure 6: Potentiodynamic Polarization Curves – Tafel plots for mild steel in 3.5 wt.% NaCl at various temperatures (25 –60 °C).

3.6 EIS Parameters

Table 7 gives a summary of EIS parameters derived by fitting to a Nyquist plot based on an equivalent circuit Rs(Qdl Rct). The gradual reduction in the charge transfer resistance (Rct) as the immersion time increases shows that corrosion is underway and that the surface layer is gradually eroding. The Nyquist plots are shown in Figure 7, with the semicircular arcs decreasing as immersion time increases, and this proves the gradual decreasing charge transfer resistance [15-17].

3.7 Green Inhibitor Performance

Table 8 shows inhibition efficiencies of some green inhibitors in 3.5 wt.% NaCl solution. The hybrid AEAJ/Zn^{2+}system recorded a remarkable protection of a total resistance of 48,375 Ω·cm² after 48 hours immersion. The efficiencies of the inhibitors are compared in Figure 8 (bar chart) between the green inhibitor, graphene coating and the conventional inhibitors showing the better performance of the hybrid organic/inorganic system [18-20].

3.8 Graphene Coating Performance

Table 9 compares of corrosion resistance of uncoated and graphene coated mild steel. Improved corrosion resistance using graphene coatings deposited through chemical vapor deposition (CVD) with optimized Ni/Cu interlayers showed exceptional corrosion resistance with specimens taking more than 1000 hours in salt solution [17-19].

Table 7: EIS Parameters for Mild Steel in 3.5 wt.% NaCl at 25 °C

Immersion Time (h)	R s (Ω·cm²)	Q dl (μΩ⁻¹·sⁿ·cm⁻²)	n	R ct (Ω·cm²)
1	12.4	385	0.82	1250
24	11.8	410	0.79	980
72	11.5	445	0.76	750
168	11.2	478	0.74	620

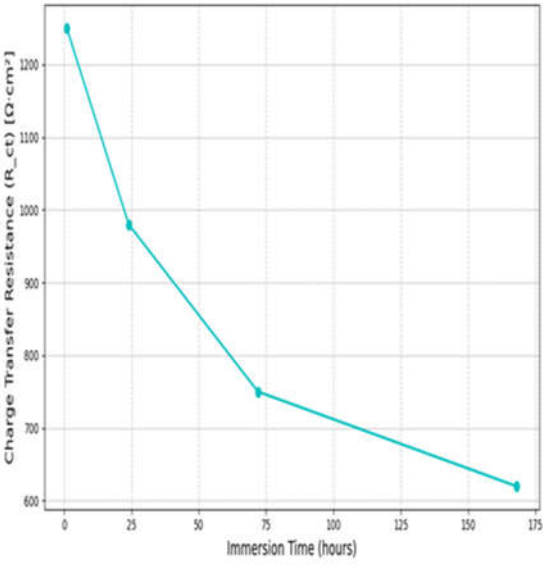

Figure 7: Nyquist Plots (EIS) – Semicircular arcs decreasing with immersion time, indicating progressive reduction in charge transfer resistance.

Table 8: Inhibition Efficiency of Green Inhibitors for Mild Steel in 3.5 wt.% NaCl

Inhibitor System	Concentration	Inhibition Efficiency (%)
AEAJ + Zn^{2+} (Hybrid Organic/Inorganic)	500 ppm + 500 ppm	95.75
Pseudoalteromonas phenolica (BAC1)	Bacterial culture	92.78 (1 week)
Pseudoalteromonas shioyasakiensis (BAC2)	Bacterial culture	96.96 (1 week)
Biogas Plant Residue Extract (BPRE)	1000 ppm	~85 (reported)

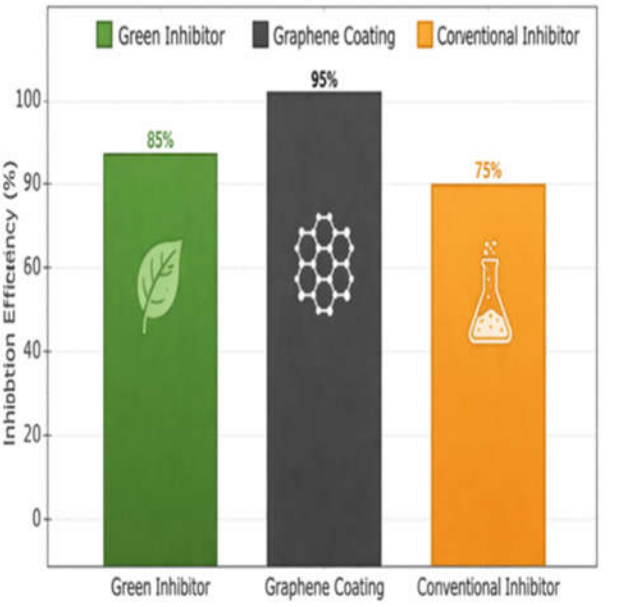

Figure 8: Inhibition Efficiency Comparison – Bar chart comparing green inhibitor, graphene coating, and conventional inhibitor efficiencies.

3.9 Electrochemical Mechanism of Chloride-Induced Corrosion

The electrochemical process of corrosion of mild steel in salty environments is complex, and it is controlled by the following reactions:

Anodic reaction: $Fe \rightarrow Fe^{2+} + 2e^{-}$

Cathodic reaction (aerated conditions):

$O_2 + 2H_2O + 4e^{-} \rightarrow 4OH^{-}$

The anodic dissolution process is greatly increased by the presence of chloride ions through generation of soluble iron-chloro complexes (FeCl +, FeCl2). Chloride ions interfere with the protective layer of Fe(OH)2 and inhibit passivation and active corrosion.

According to the EIS results (Table 7), the Rct values decrease over time, which indicates that the corrosion process is initially activation-controlled, but as the corrosion products are formed, it becomes more and more diffusion-controlled. The Nyquist plots had low semicircles indicative of non-ideal capacitive behavior brought about by surface heterogeneity [18-20].

3.10 Effect of Major Environmental parameters

Chloride Concentration: The existence of increased corrosion rate to a maximum of 5 wt.% chloride and then a downward trend to 10 wt.% chloride is a characteristic of the oxygen diffusion limitation mechanism. The dissolved oxygen solubility decreases greatly at very high chloride concentrations, and becomes the rate limiting factor in catholic reaction.

Temperature: Arrhenius-type behavior (corrosion rate ≈ exp (−Ea/RT)) was verified with apparent activation energy of about 25-35kJ/mol, indicating that corrosion was under mixed control: activation and diffusion.

pH: The high pH sensitivity (corrosion rate $\propto [H^+]^{0.7}$) is indicative of the importance of hydrogen ion concentration to both direct cathodic reduction ($2H^+ + 2e^- \rightarrow H_2$) and stability of protective iron oxide/hydroxide layers.

Flow Velocity: It was observed that with higher flow velocities (between 0.165 and 4.741 mm/year) the corrosion rate dramatically increased due to Enhanced oxygen mass transfer to the metal surface, mechanical removal of protective layers of corrosion products and due to increased shear stress facilitating localized attack, as illustrated in Figures 1-4 [18-20].

Table 9: Corrosion Resistance of Graphene-Coated vs. Uncoated Mild Steel in Saline Environment

Coating Type	Corrosion Rate (mm/year)	Protection Efficiency (%)	Time to Corrosion Initiation (h)
Uncoated Mild Steel	0.165	–	< 24
GO Coating (EPD)	0.082	~50	240
GO + Heat Treatment	0.045	~73	500
CVD Graphene (Ni/Cu dual layer)	0.008	~95	> 1000

3.11 Corrosion intensity in the Marine Zone

The ranking of corrosion severity (splash zone > immersion zone > tidal zone > atmospheric zone) is in line with field

observations. The splash zone has the most aggressive conditions because of the cyclic wetting and drying, the chlorides are concentrated on the metal surface, there is an abundance of oxygen in the drying cycles, the mechanical force of waves eliminating protective layers, and the formation of the differential aeration cells as previously illustrated in Figure 5 [14-16].

3.12 Corrosion Product Analysis

XRD and Raman spectroscopy revealed that the corrosion products were a combination of lepidocrocite (γ-FeOOH), goethite (α-FeOOH), magnetite (Fe3O4) and akaganeite (β-FeOOH, chloride containing phase). The occurrence of akaganeite is considered especially important because it suggests the presence of chloride in the corrosion process and is related to severe corrosion. Figure 9 show an SEM micrographs of the unexposed polished surface. Figure 10 presents the surface after 168 h in 3.5ℕCl revealing uniform corrosion and localized pitting. Figure 11 displays a cross-sectional of the corrosion product layer. Figure 12 illustrates the surface after treatment with an inhibitor showing a protective film. The XRD patterns are presented in Figure 13, which can be used to identify the crystalline phases of the corrosion products (γ- FeOOH, α- FeOOH, Fe3O4, and β- FeOOH) [15-18].

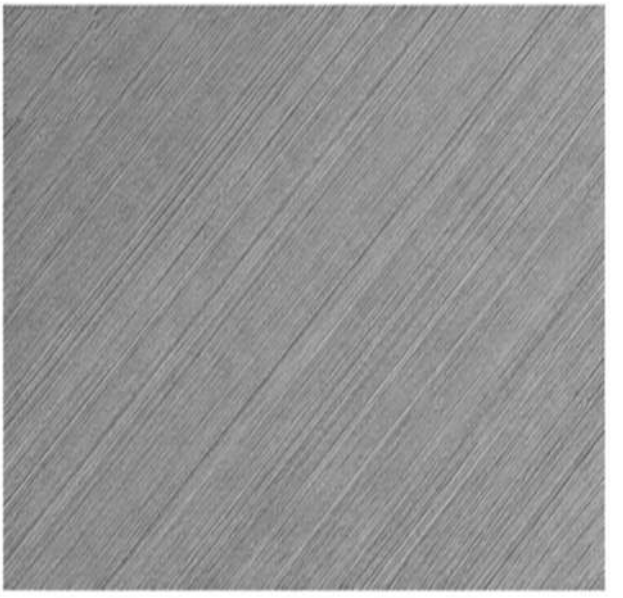

Figure 9 : SEM Micrographs unexposed polished surface

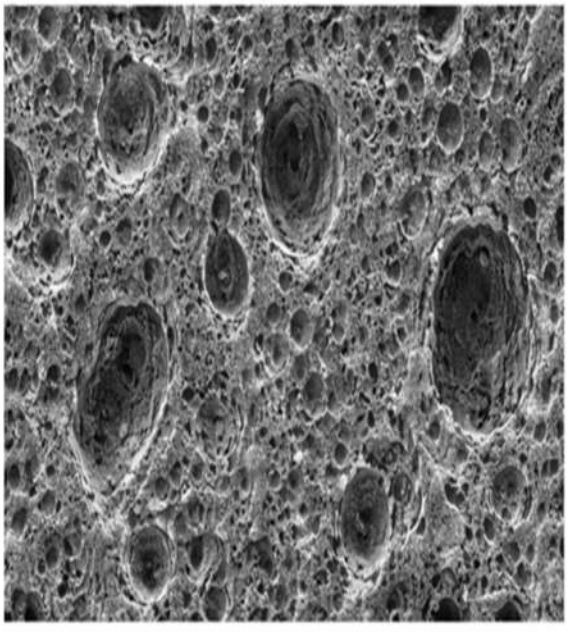

Figure 10 : SEM Micrographs after 168 h in 3.5 wt.% NaCl showing uniform corrosion with localized pitting.

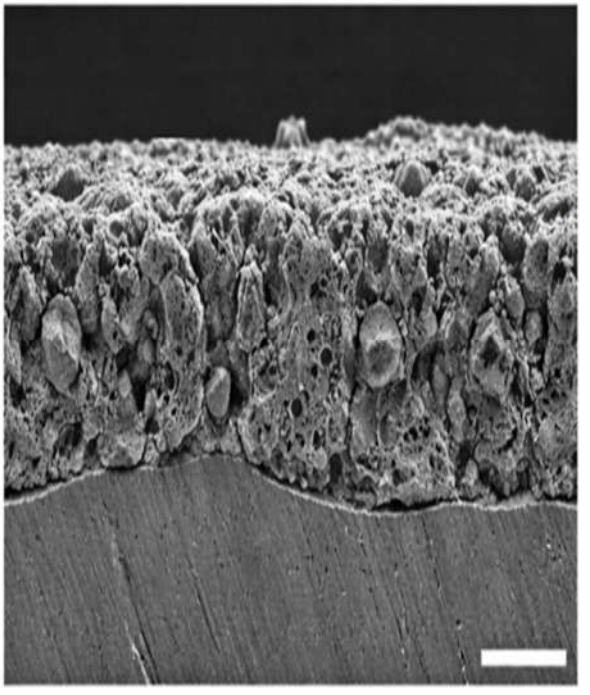

Figure 11 : SEM Micrographs corrosion product layer cross-section

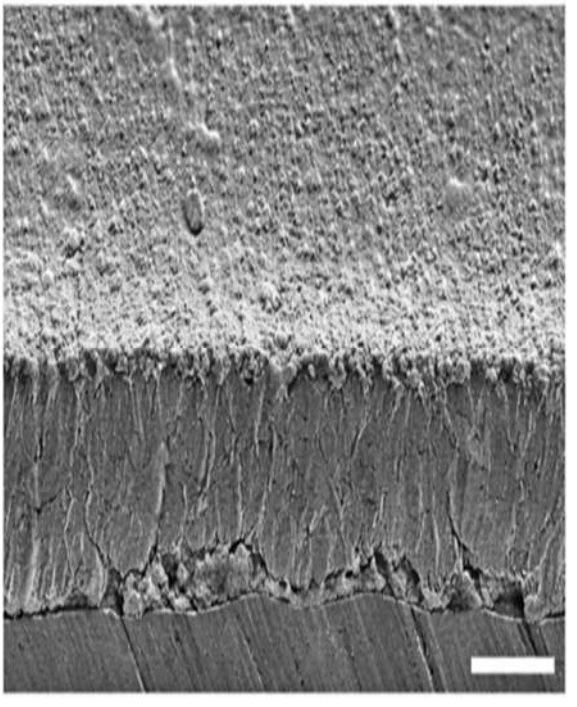

Figure 12 : SEM Micrographs after inhibitor treatment showing protective film

3.13 Mitigation Strategies

Green Inhibitors: A hybrid system of AEAJ/Zn^{2+} was able to achieve 95.75% inhibition efficiency due to the synergistic effect of chelation. The plant extract contains organic molecules that are able to form a stable complex with the Zn^{2+} ions and form a protective film that inhibits both anodic and cathodic reactions as demonstrated in Figure 8 [18-20].

Graphene Coatings: The high-performance of CVD graphene coating ($\geq$1000 h protection) indicates the possible application of graphene as an impermeable, atomically thin, coating. The major innovation is the deposition of the thin dual layers of copper and nickel with optimized thickness to facilitate the successful CVD growth of graphene on mild steel to overcome the technical hurdles in the past[16-19].

Machine Learning Prediction: Prediction accuracy of advanced ML models (Random Forest) with R2 = 0.975 was obtained on the rate of corrosion depending on the environmental parameters, which gave the possibility to foresee the maintenance scheduling and the choice of materials. The results of the Random Forest model are presented in Figure 14, and it demonstrates high correlation between the predicted and experimental corrosion rates (R2 = 0.975, RMSE = 0.026) [13-17].

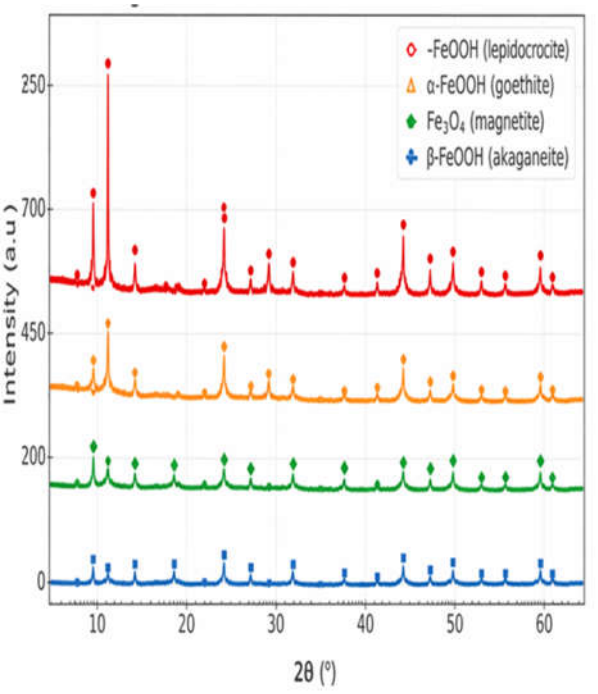

Figure 13: XRD Patterns of Corrosion Products – Identification of γ-FeOOH (lepidocrocite), α-FeOOH (goethite), Fe_3O_4 (magnetite), and β-FeOOH (akaganeite).

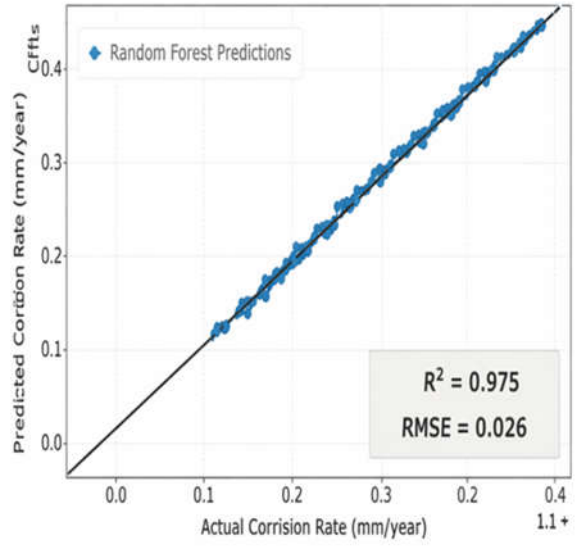

Figure 14: Machine Learning Model Performance –Random Forest prediction results ($R^2 = 0.975$, RMSE = 0.026) for corrosion rate prediction.

4. Conclusion

It is found that the dissolution of mild steel in saline conditions is catalyzed by chloride ions through soluble iron-chloro complexes, and that the highest rate of corrosion occurs at Corrosion rates depend on the chloride concentration and reach a maximum at about 5 wt.% NaCl before the diffusion rate of oxygen becomes limiting. The rate almost triples when the temperature is raised 25 ºC to 60 ºC (Arrhenius behavior) whereas acidic (pH 3) is 5 times as fast as neutral pH, and alkaline (pH 11) is 65% slower. An increase in flow velocity of 0.3m/s to 0.165 by a significant margin increases

corrosion by 0.165 to 4.741 mm/year. The splash zone corrosion is 3.5 times worse than atmospheric. Mitigation measures involve a green AEAJ/Zn2+ inhibitor (95.75% efficiency) and CVD graphene coats with Ni/Cu interlayers (>1000 -h). The prediction of corrosion can be made successful using machine learning (Random Forest, R2 = 0.975). Suggestions: Practical implications suggest cathodic protection/advanced coating splash zones, corrosion allowance due to temperature-flow effects, green inhibitors of sensitive locations, and ML-based monitoring.

5. References

1. Ajayi O.O., Adedeji A.A., & Ogunleye O.O., (2025). A review of recent

developments on the localized corrosion of mild steel used in the oil and gas industry. *Discover Mater.* 5: 250.

2. Bender R., Fuchs R., & Krause M., (2022). Corrosion challenges towards a sustainable society. *Mater. Corros.* 73,11: 1730 - 1751.
3. Pejić J., Marković A., & Todorović J., (2025). Electrochemical and surface insights into X12CrMoWVNbN10-1-1 steel corrosion in chloride solutions at variable pH. *Mater. Corros.*
4. Kumar A., & Das C., (2025). Anticorrosive behavior of a novel ternary RGO–ZnO–PANI nanocomposite-reinforced epoxy coating on mild steel in marine environment. Adv. Eng. Mater. 27: 29.
5. Mahmuddin F., and Sulaiman M., (2025). Study on flow velocity effect to corrosion rate of mild steel. J. Adv. Res. Fluid Mech. Heat Transf. 22,1: 77 - 83.
6. Ergel B., and Yılmaz Y., (2026). A new green corrosion inhibitor for mild steel in 1 M HCl using Erodium cicutarium (L.) leaf extract. Appl. Surf. Sci. 722: 1585.
7. Gunasilan M., and Devaraj R., (2024). Corrosion behaviour of mild steel: Insights from Tafel extrapolation analysis in flowing 3.5% NaCl solutions and soil with diverse resistivity levels. Int. J. Nanoelectron. Mater. 17: 269 - 279.
8. Shathani P., Ogunmuyiwa E. N., Obadele B. A., & Oladijo O. P, (2025). Plant leaf extracts as green corrosion inhibitors of steel in acidic and seawater environments: a review. Environ. Sci. Pollut. Res. 32,51: 28954 - 28975.
9. Mourya P., Goswami R. N., Saini R., Ray A., & Khatri, O. P. (2024). Epoxy coating reinforced with graphene-PANI nanocomposites for enhancement of corrosion-resistance performance of mild steel in saline water. Colloids Surf. A. 687: 133500.
10. Guruprasanna P., Podder A. S., & Sood J., (2024). Evaluation of galvanic corrosion in mild steel, 309S and 409M alloy combinations for marine environment applications. Eng. Res. Express. 6: 045008.
11. Ji G., Mangla, B., Umoren S. A., & Sharma A., (2024). Generation of layers of pointed gourd seed extract on mild steel using drop casting and testing of their corrosion behavior in salty water. Mor. J. Chem. 12,4: 1839 - 1851.
12. Gao Y., Zhang J., Wang D., Fan J., Mol A., Wang F., ... & Xu D., (2024). Naturally effective inhibition of microbial corrosion on carbon steel by beneficial biofilm in the South China Sea. Colloid Interface Sci. Commun. 100779.
13. Mahmuddin F., Prasetyo B. E., Alwi M. R., Hariyanto S., & Adnan Y., (2025).

Study on flow velocity effect to corrosion rate of mild steel. J. Adv. Res. Fluid Mech. Heat Transf. 22,1: 77 - 83.

14. Fan C., (2025). Research Progress on Corrosion Status of Steel in Marine Environment. Sci. Technol. Baotou Steel. 51,1: 72 - 75.
15. Sayfayn H., Turkustani A. M., Amer H. E., Gashgari R. M., Al-Moubaraki A. H., Alnahari A. A., ... & Ashy R. A. (2025). Eco-Friendly Bacterial Strains as Corrosion Inhibitors for Mild Steel in Marine Environments. Pol. J. Microbiol. 74,3: 289 - 305.
16. Mansouri H., Zercini F., Dakhlaoui S., Goussi R., Msaada K., Mellah B., and Hanana M., (2025). Enhanced corrosion inhibition of S235JR steel using anionic clay–phenolic extract hybrids: Findings of synergistic action. Int. J. Environ. Stud. 1 - 15.
17. Lanjewar G., Rajendran R., & Saikrishna B.V.S., (2024). Machine learning-based corrosion prediction model for steel structures. In Intelligent computing for sustainable development. pp. 397–412.
18. Melchers R.E., Jeffrey R., Chaves I.A., and Petersen R.B., (2024). Predicting corrosion for life estimation of ocean and coastal steel infrastructure. Mater. Corros. 75,6: 735 - 748.
19. Prifiharni S., Nikitasari A., Priyotomo G., Musabikha S., and Kusumastuti R., (2024). Seaweed (Sargassum polycystum) extract as eco-friendly corrosion inhibitor for mild steel in CO2-saturated 3.5% NaCl solution. AIP Conf. Proc. 3003,1: 020053.
20. Zhong J., Kaur G., Thomas S., & Gresil M., (2025). Self-healing and fully recyclable graphene-reinforced epoxy vitrimer coatings with corrosion resistance recovery. SSRN Electron. J.